Optical Materials 147 (2024) 114615

Contents lists available at ScienceDirect

Optical Materials

journal homepage: www.elsevier.com/locate/optmat

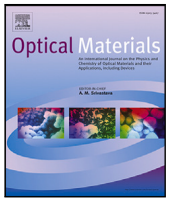

Research article

Optically transparent dual-band antenna for UHF and S-band applications

Eknath C. Patil [a,1], Shashikant D. Lokhande [a,1], Uday A. Patil [b,1], Atula U. Patil [c,1], Jayendra Kumar [d,*,1]

[a] Electronics and Telecommunication Engineering Department, Sinhgad College of Engineering, SPPU, Pune, Maharashtra 411041, India
[b] Department of Technology, Shivaji University, Shivaji University, Kolhapur, Maharashtra 416004, India
[c] Department of Physics, Rajaram College, Kolhapur, Maharashtra 416004, India
[d] School of Electronics Engineering, VIT-AP University, Inavolu, Andhra Pradesh 522 237, India

ARTICLE INFO

Keywords:
Dualband antenna
ITO-PET
SLG substrate
Transparent antenna
Wideband antenna

ABSTRACT

This paper presents a novel optically transparent antenna that utilizes Indium Tin Oxide-coated Polyethylene Terephthalate (ITO-PET) and Soda-lime-glass (SLG) substrate. It explores ITO-PET and SLG for transparent antenna fabrication, thoroughly evaluating the antenna's performance in relation to ITO-PET's conductivity. Operating in dual bands (1.6–2 GHz UHF and 3.25–4.95 GHz S-band), the antenna's inventive design features a slotted circular structure with a modified ground plane, crucial for achieving dual-band functionality. Despite ITO-PET's relatively low conductivity, the antenna outperforms expectations, exhibiting a wider bandwidth in the higher band and positive gain in both bands, conforming the potential of ITO-PET. The successful realization of this innovative concept is validated through the fabrication and measurement of the antenna prototype, signaling a new frontier in transparent antenna technology.

1. Introduction

Transparent components facilitate the creation of flexible [1], and wearable electronics, enabling comfortable integration into clothing and accessories [2]. Transparent electronics components are crucial for Augmented Reality (AR) and Virtual Reality (VR) applications, where digital information is overlaid on the real-world view [3]. An antenna is a crucial component in electronics that plays a fundamental role in both sending and receiving signals, particularly in the context of wireless communication. Antennas enable wireless communication by converting electrical signals into electromagnetic waves that can propagate through the air or other mediums. They facilitate the transmission of information, such as voice, data, and video, over long distances without the need for physical cables. Thus the devolvement of transparent antennas are need for the current future generation of transparent electronics circuits.

The Cellular Telecommunications and 5G network operates in 900–2100 MHz and 3500 MHz frequency bands, respectively and provides many communication services. The transparent antenna technology allows for the deployment of high-frequency antennas in everyday objects like windows [1], smart glasses [4], or even in the screens of mobile devices, without compromising the aesthetics or visibility. By blending seamlessly with the environment, transparent antennas offer the potential to enhance cellular network coverage and capacity in urban areas while minimizing visual and structural intrusiveness. As the demand for high-speed, high-capacity mobile data continues to grow, transparent antennas pave the way for improved connectivity and a harmonious coexistence of telecommunications infrastructure with the architectural and aesthetic demands of modern urban landscapes.

A transparent antenna refers to an antenna that is designed and constructed in such a way that it is nearly invisible or minimally obtrusive when placed on or integrated into transparent or translucent materials, such as glass or plastic. These antennas are often used in applications where aesthetics or design considerations are important, and traditional visible antennas would be undesirable. Transparent antennas find applications in various industries, including automotive, architecture, consumer electronics, and more. Many transparent antennas have been reported in the literature constructed using different transparent material [5–16]. In [5], transparent antenna is fabricated using a soda-lime glass (SLG) substrate with fluorine doped conductive oxide (FTO) for energy harvesting applications. The antenna operates from 2 to 6 GHz, featuring enhanced impedance bandwidth using a radial stub. With a directional radiation pattern, it achieves a peak gain of 2.5 dBi at 4 GHz and over 28% radiation efficiency. In [6], The choice for conductors in the wearable glasses involves a multilayer electrode film comprising transparent conducting oxide electrodes, specifically 100-nanometer-thick indium–zinc–tin oxide (IZTO)/Ag/IZTO (IAI), serving

* Corresponding author.
E-mail addresses: jayendra854330@gmail.com, kumar.jayendra@vitap.ac.in (J. Kumar).
[1] All authors have contributed equally to this work.

https://doi.org/10.1016/j.optmat.2023.114615
Received 7 September 2023; Received in revised form 9 November 2023; Accepted 15 November 2023
Available online 23 November 2023

Table 1
Performance of circular patch antenna against conductivity.

Material	f_0 (GHz)	Bandwidth (MHz)	Gain (dBi)	Radiation efficiency (%)	FBR (%)
Copper	2.45	142	6.3	98.54	92.17
ITO	2.38	150	−1.3	48.32	87.21

as the antennas and ground planes. In [7], authors have a novel concept: a transparent halved coplanar Vivaldi antenna (HCVA) operating in the ultrawideband (UWB) range. The innovation lies in the incorporation of a metal mesh film (MMF) which possesses exceptional attributes - a minimal sheet resistance of 0.35 Ω/sq and remarkable optical transmittance exceeding 72% for both the radiation fin and the ground plane. This strategic integration of the MMF engenders a fully transparent antenna system. Similarly, in [8,9], MMF is used to develop a transparent patch antennas. AghT-8 transparent thin film is used in [10] to develop an ultra-wideband (UWB) antenna. In [11], authors have used silver grid layer (AgGL) deposited on one side of Corning glass substrate. The multilayer antenna's theoretical optical transparency spans from 51.6% to 70.7% across the entire range of visible light wavelengths. In [12], authors have reported an adaptable UWB antenna characterized by its transparency. The antenna employs a polydimethylsiloxane (PDMS) substrate adorned with a transparent conductive fabric. The fabrication process involves affixing a layer of this conductive fabric to both the upper and lower surfaces of the PDMS, resulting in a tri-layer fabric panel. The subsequent step entails the precise formulation of radiating elements on the top and bottom layers through the utilization of a laser machine. [13] presents a thin film-based transparent antenna targeted for solar cells. Annealing processes were conducted on GZO thin films to enhance their suitability for transparent antenna applications. As a result of the annealing treatment: Both microstructural and optoelectronic characteristics exhibited noticeable enhancements and also, annealed GZO thin films present a versatile option for crafting antennas tailored to various applications. In [14–16] AgHT-4/8 conductive oxide material is used to realize wideband transparent antennas.

This study introduces an innovative concept in the realm of optically transparent antennas by utilizing Indium ITO-PET in combination with a SLG substrate. The unique approach involves a comprehensive exploration of ITO-PET and SLG materials for transparent antenna construction. The research delves the antenna's operational performance, particularly analyzing the conductivity attributes for antenna applications. Operating within dual frequency bands, the antenna's architecture features slotted circular structure, complemented by a modified ground plane. This structural adaptation plays a pivotal role in realizing the antenna's dual-band functionality, marking a significant novelty. Notably, it exhibits an expanded bandwidth within the higher frequency band and showcases positive gain across both frequency ranges. This outcome emphatically underscores the potential of ITO-PET for microwave applications. The experimental results of this work is substantiated through the meticulous fabrication and precise measurement of a prototype antenna. This pivotal milestone heralds the advent of a fresh frontier in transparent antenna technology, signifying an advancement in the field.

2. Antenna design

This section presents an analysis of the performance of the patch antenna in relation to the conductivity of both the patch material and ground plane. The purpose of this analysis is to provide a better understanding of the antenna's performance by comparing it to a traditional circular patch antenna. Additionally, the layout, numerical simulation, and analysis of the proposed transparent dual wideband antennas are presented.

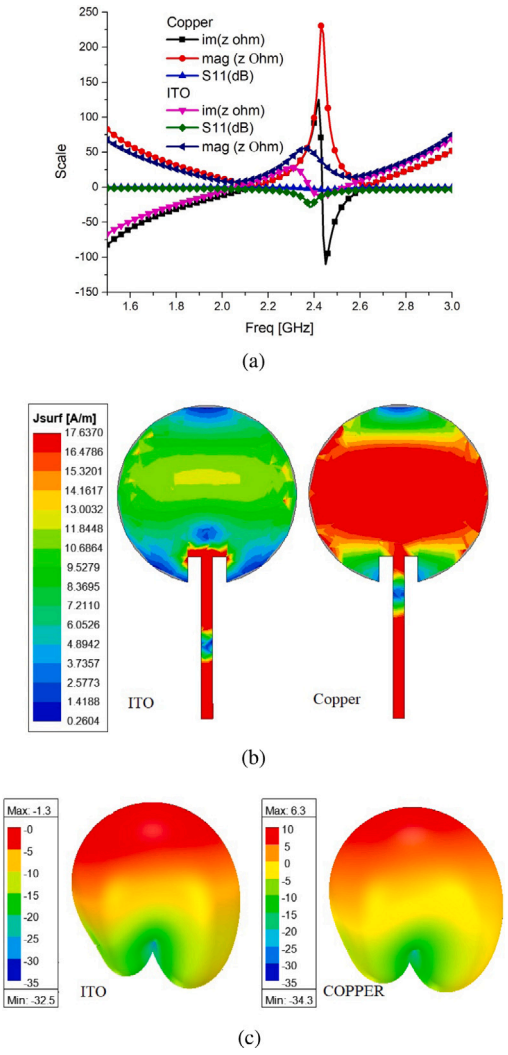

Fig. 1. Performance of circular patch antenna against conductivity of the patch and ground plane (a) Impedance matching parameters (b) Surface current distribution (c) 3D gain total (dBi).

2.1. Conductivity analysis

The objective of this research is to develop an optically transparent patch antenna. However, the conductivity of various conductive transparent materials is significantly lower than commonly used metals such as copper and aluminum. Therefore, it is crucial to examine the performance of a conventional patch antenna when using a lower conductivity patch and ground plane. In this study, we utilize Indium Tin Oxide coated Polyethylene Terephthalate (ITO-PET) with a sheet resistivity of 10 Ω/sq as both the patch and the ground plane. We design a conventional inset feed circular patch antenna that operates at the Industrial, Scientific, and Medical (ISM) frequency of 2.4 GHz. Subsequently, we investigate its performance in relation to the conductivity of the ITO-PET material (45 000 s/m) and copper (5.8×10^6 s/m).

Fig. 1 illustrates the impedance matching parameter, surface current distribution, and three-dimensional total gain of the 2.4 GHz ISM band antenna. Table 1 presents additional performance metrics. The conductivity of the patch and ground has a significant impact on impedance matching and radiation performance. In Fig. 1(a), it is evident that the copper-based antenna exhibits higher input impedance at the same inset feed position compared to the ITO-based antenna. However, by adjusting the inset feed position, impedance matching can be achieved.

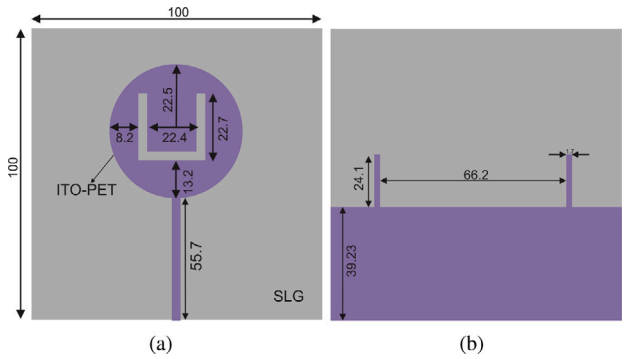

Fig. 2. Layout of the proposed transparent antenna (circular patch radius 22.7 mm and U-slot width 2.8 mm) (a) Top view (b) Bottom view (Units mm).

The research findings presented in [17] indicated that while conductivity had no impact on the absorption efficiency of certain antennas, the absorption cross-sectional characteristics of these antennas correlated with the radiation efficiency. For the proposed antenna structure a higher conductivity materials exhibit a sharp transition from inductive reactance to capacitive reactance at the resonance frequency, unlike low conductivity materials. This is due to the mismatch between the characteristic impedance and the impedance of the designed antenna for the same feeding position. Fig. 1(b) demonstrates that the ITO-PET patch accumulates lower surface current compared to the copper patch due to its lower conductivity. Consequently, the radiation efficiency is adversely affected, as depicted in Fig. 1(c). The ITO-PET-based antenna has a significantly lower antenna gain of −1.3 dBi, whereas the copper-based antenna has a gain of 6.3 dBi. Table 1 further highlights that the ITO-PET antenna resonates at a lower frequency. ITO-PET exhibits reduced sheet resistance, resulting in a lower resonant frequency. Moreover, when comparing antennas of equal dimensions, the ITO-PET-based antenna exhibits a lower resonant frequency compared to copper-based antennas. In the case of a patch antenna, a higher dielectric constant substrate leads to a lower operating frequency and broader bandwidth. Consequently, an ITO-PET-based antenna demonstrates a response close to a patch antenna constructed on a substrate with a higher dielectric constant. This characteristic is attributed to the integration of the thick, low conductivity ITO-PET material. Although the bandwidth is wider for the ITO-PET-based antenna, its radiation efficiency and front-to-back ratio (FBR) are poorer, as mentioned in Table 1.

2.2. Antenna layout

Fig. 2 presents the layout of the proposed antenna. The antenna has been designed using a transparent Soda Lime Glass (SLG) substrate, which not only provides structural support but also offers excellent optical properties for transparency. The SLG substrate boasts specific attributes, including a thickness of 1 mm, a dielectric constant of 3.2, and a dielectric loss tangent of 0.02, all of which significantly influence the antenna's electrical behavior. Complementing the SLG substrate, the antenna features a transparent conductive ITO-PET (Indium Tin Oxide on Polyethylene Terephthalate) patch and ground plane. This combination of materials ensures efficient radiation while maintaining optical transparency. The conductive ITO-PET patch, with a sheet resistance of 10 Ω/Sq. and a slim thickness of 0.7 mm, allows for precise control of the antenna's electromagnetic properties. As a result of the careful selection and integration of these materials, the overall thickness of the antenna is finely tuned to a mere 2.4 mm.

The structure of the antenna comprises several key elements, each contributing to its performance. A conductive slotted circular patch forms the primary radiating element. This circular patch is loaded with a U-shaped slot strategically positioned in both the X and Y directions. This asymmetrical arrangement of the U-shaped slot, deliberately shifted by 2 mm towards the negative X-direction and by 1.5 mm towards the negative Y-direction relative to the center of the circular patch, enables precise control over the antenna's radiation pattern and impedance characteristics. To expand the antenna's operational range and attain wider bandwidth, a modified ground plane incorporating a U-shaped parasitic element has been employed. This partial ground plane, known for its capability to produce wideband and omnidirectional radiation patterns, is integrated with two stubs and a U-shaped parasitic element identical to the patch slot. By positioning this parasitic element just beneath the circular patch, additional benefits are achieved. The development of this antenna involves an rigorous optimization process that employs the Ansys Full-wave Electromagnetic simulator. Through thorough examination and fine-tuning of the dimensions of the slots, partial ground, integrated stubs, and U-shaped parasitics, the antenna's performance in the UHF and S-band is tailored to deliver wider bandwidth and quasi-omnidirectional radiation characteristics. In the subsequent sections of this work, a detailed and comprehensive analysis of the antenna's design, along with insights into the optimization process, have been presented.

2.3. Numerical simulation and analysis

In this section, we delve into the fundamental design parameters of the antenna structure, aiming to pinpoint their significance concerning antenna impedance matching and radiation pattern.

The objective is to enhance our understanding of the antenna's behavior and performance under different modifications. The antenna under study is a circular patch antenna, which has undergone three major modifications to improve its characteristics. These modifications encompass the integration of a U-shaped asymmetrical slot into the circular patch, the truncation of the ground length, and the addition of two rectangular stubs to the truncated ground plane. Each of these alterations plays a crucial role in shaping the antenna's behavior, and their effects are meticulously examined and presented in the subsequent discussions.

First we focus on the impact of ground length truncation on the antenna's bandwidth and radiation pattern in both the E-plane and H-plane, as illustrated in Fig. 3. It becomes evident that the ground length has a minor effect on the lower frequency band but exerts a significant influence on the bandwidth of the higher operating band, as demonstrated in Fig. 3(a). In other words, adjusting the ground length allows for control over the antenna's frequency response, particularly in the higher frequency range. Conversely, the radiation pattern and gain of the lower frequency band are greatly affected by variations in the ground length, as depicted in Fig. 3(b). This indicates that the ground length is a critical parameter in shaping the antenna's radiation characteristics, especially at lower frequencies. The radiation pattern of the higher frequency band remains relatively unaffected by changes in the ground length, as revealed in Fig. 3(c). This suggests that other design parameters or modifications may play a more dominant role in determining the radiation pattern at higher frequencies.

The influence of the U-shaped asymmetrical slot on both antenna impedance matching and bandwidth is comprehensively explored in Fig. 4. We delve into the details of each parameter and its impact on the antenna's performance. Starting with the slot width, Fig. 4(a) showcases its effect on the antenna. The slot width has a relatively minor influence on the antenna's bandwidth; however, it does affect the impedance matching in the lower frequency band. Although there is some deviation in impedance matching, the S11 parameter remains well below −10 dB, indicating that the antenna's performance is still suitable for practical applications. Moving on to the slot length, as demonstrated in Fig. 4(b), it becomes evident that this parameter plays a more significant role in shaping the higher cut-off frequency of the lower band. Adjusting the slot length allows fine-tuning the

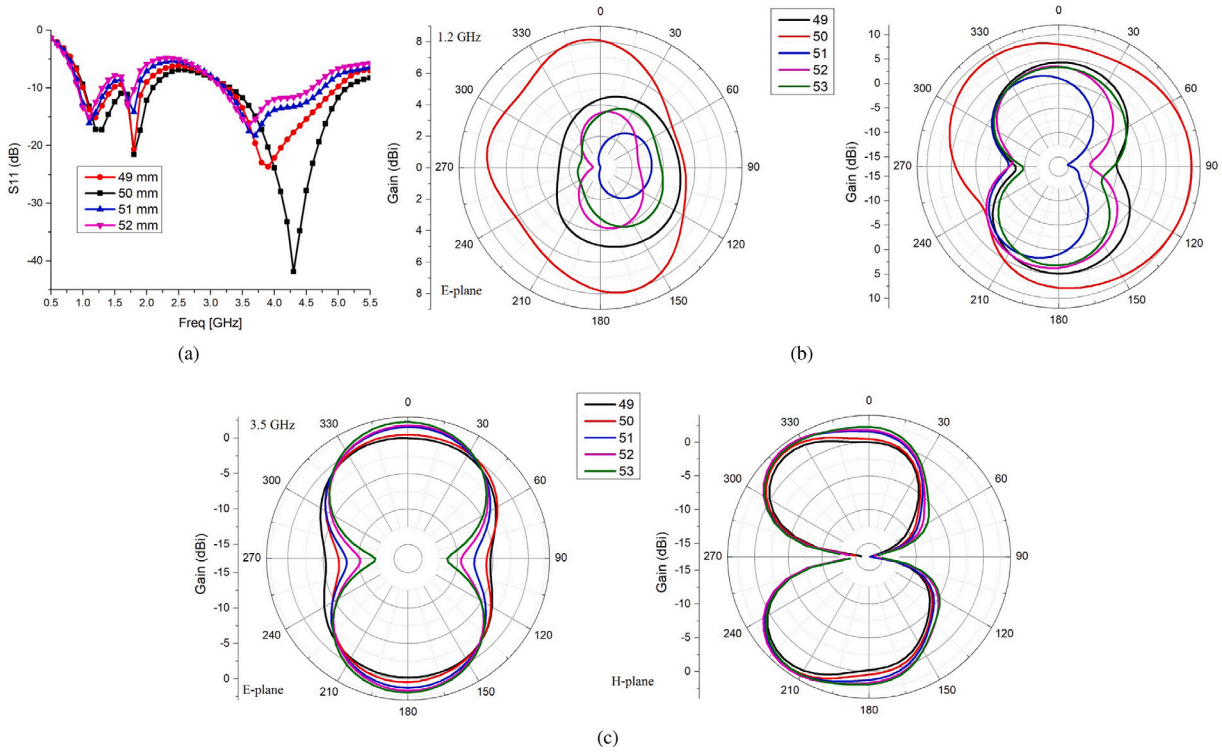

Fig. 3. Parametric analysis of partial ground length on (a) Scattering parameter (b) Radiation pattern at 1.2 GHz (c) Radiation pattern at 3.5 GHz.

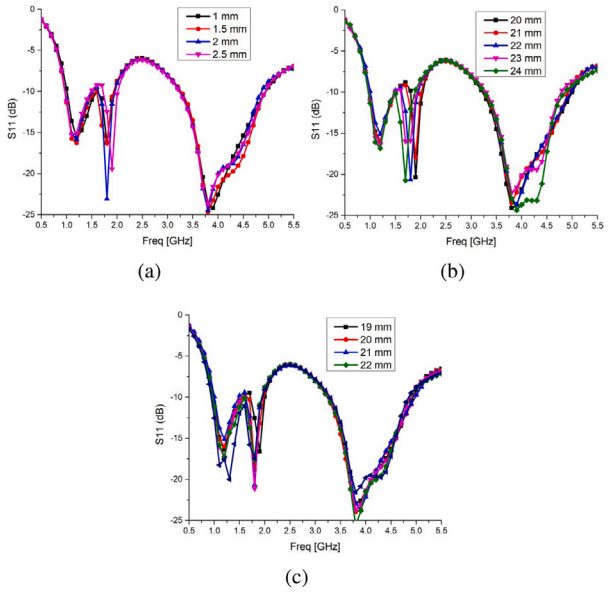

Fig. 4. Parametric analysis of patch slot on scattering parameter (a) Against slot width (b) Slot length (c) Slot position.

antenna's frequency response, especially in the lower frequency band. The slot position also exerts an impact on the lower band, as depicted in Fig. 4(c). By strategically choosing the slot position, it is possible to achieve desired changes in the antenna's impedance matching and bandwidth within the lower frequency range. The incorporation of the U-shaped asymmetrical slot into the circular patch presents a promising approach to control the bandwidth and impedance matching of the lower frequency band. Fine-tuning the slot width, length, and position offers valuable opportunities for customizing the antenna's performance to meet specific application requirements.

The impact of the patch slot length on the radiation pattern in both operating bands is the subject of investigation, visually presented in Fig. 5. The findings reveal that the slot length exerts a particularly strong influence on the radiation pattern within the lower frequency band, as depicted in Fig. 5(a). By controlling the slot length, it becomes feasible to achieve either a perfect endfire pattern or an omnidirectional E-plane pattern. This versatility is clearly evident in Fig. 5(b), where a slot length of 24 mm results in an endfire radiation pattern at the frequency of 1.2 GHz, while slot lengths below 24 mm lead to an omnidirectional pattern. In contrast, the effect of slot length on the higher frequency band is comparatively minor, implying that variations in the slot length have less pronounced consequences in this range.

The modifications made to the ground plane wield a substantial influence over the bandwidth, impedance matching, and gain of the upper frequency band. A comprehensive analysis of the ground stubs parameter and the antenna input scattering parameter is presented in Fig. 6, shedding light on their implications. By adjusting the stub width, we can finely tune the upper cutoff frequency of the higher frequency band, as shown in Fig. 6(a). Similarly, change of the stub length permits precise fine-tuning of the lower cutoff frequency within the higher frequency band, as depicted in Fig. 6(b). While these stubs exhibit limited influence over the bandwidth or impedance matching of the lower band, extreme cases demonstrate a severe impact on the impedance matching in both the lower and upper frequency bands, as illustrated in Fig. 6(c). It becomes evident that the positioning of the stubs plays a critical role in shaping the antenna's performance across frequency ranges. Furthermore, the slot position emerges as a significant determinant affecting the bandwidth of the upper band. This finding shows the importance of carefully considering the slot's placement to achieve desired performance characteristics. By studying these ground plane modifications and their diverse impacts on the antenna's behavior, we can gain valuable insights into optimizing its performance across multiple frequency bands.

The ground stubs has significant influence over the antenna pattern and gain characteristics within both operating bands, as clearly illustrated in Figs. 6, 7, and 8. The width of these stubs exerts a substantial

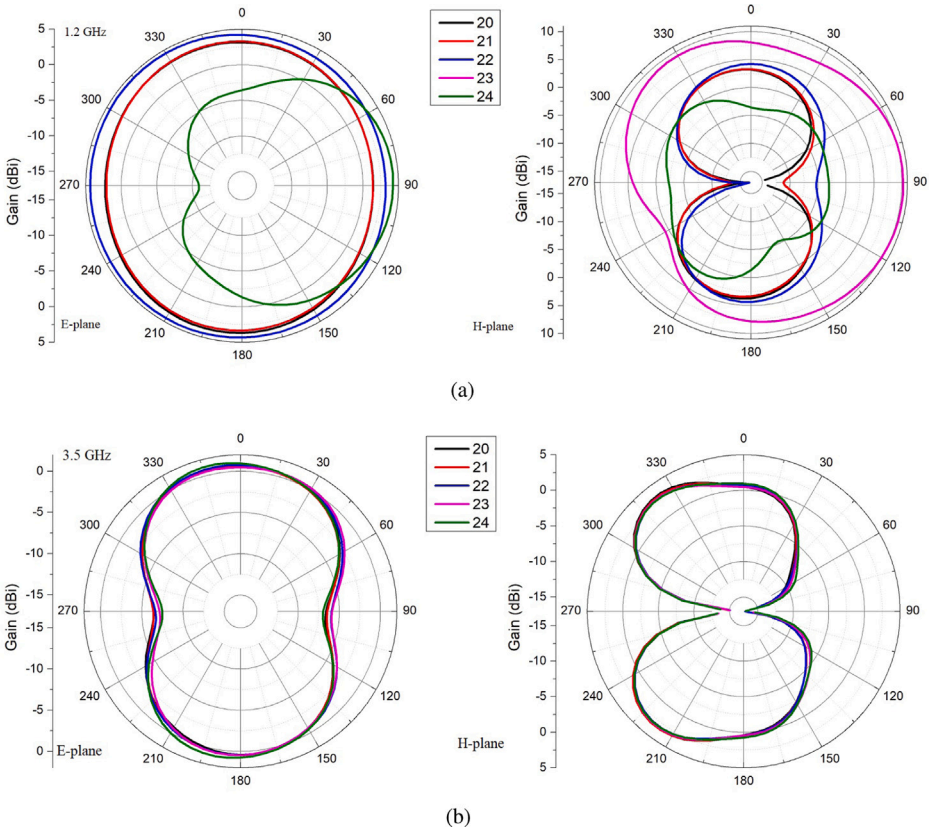

Fig. 5. Parametric analysis of patch slot length on radiation pattern (a) 1.2 GHz (b) 3.5 GHz.

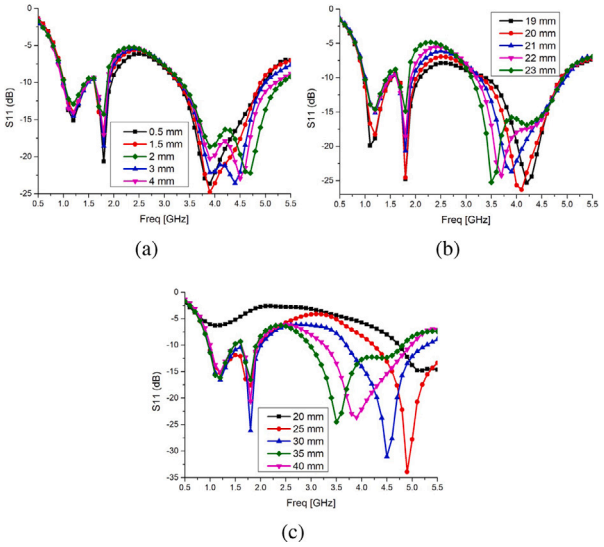

Fig. 6. Parametric analysis of ground stubs on scattering parameter (a) Stub width (b) Stub length (c) Stub position.

effect on the amplitude of the antenna's gain. Consequently, careful consideration must be given to selecting an appropriate stub width to achieve the desired antenna gain performance. It is noteworthy that this effect on gain amplitude is observed in both the E-plane and H-plane for both operating bands. This similarity in the influence of stub width on the gain characteristics across different planes underlines the importance of optimizing the stub dimensions to ensure optimal performance in both horizontal and vertical directions. By closely studying the behavior of the ground stubs and their impact on the antenna's pattern and gain, valuable insights can be gained, enabling us to fine-tune and optimize the antenna design for improved performance in the target frequency bands. The figures presented in Fig. 7 illustrate a comparative analysis of the radiation patterns between an antenna and a ground stub. Upon careful examination of Fig. 7(a), a significant observation can be made: the manipulation of the stub length allows for the attainment of either a high-gain endfire pattern or a low-gain omnidirectional pattern in the lower frequency band. Moreover, Fig. 7(b) presents analogous outcomes for the upper frequency band, whereby we can achieve a high-gain directional pattern or a low-gain omnidirectional pattern. These figures highlight the vital role that stub length plays in influencing the radiation characteristics of the antenna, providing engineers and researchers with valuable insights for optimizing performance across different frequency bands. By strategically adjusting the stub length, one can tailor the antenna's radiation pattern to meet specific communication requirements.

The positioning of the ground stub plays a pivotal role in shaping the radiation pattern across both operational frequency bands, as visually illustrated in Fig. 8. Its strategic placement wields the power to establish either an all-encompassing omnidirectional pattern or a focused endfire configuration within the lower operational band, as depicted in Fig. 8(a). Conversely, within the higher operational band, this ground stub positioning exerts a substantial influence, notably impacting the directivity along the horizontal plane (H-plane) as well as the overall gain in both the horizontal and vertical planes. This intricate interplay is vividly presented in Fig. 8(b).

3. Prototyping and validation

To develop a transparent antenna, ITO-PET is used as a radiator and the ground plane. ITO-PET comprises an Indium Tin Oxide (ITO) layer deposited onto a Polyethylene Terephthalate (PET) substrate. ITO, a transparent conductive oxide composed of indium oxide (In_2O_3) and tin

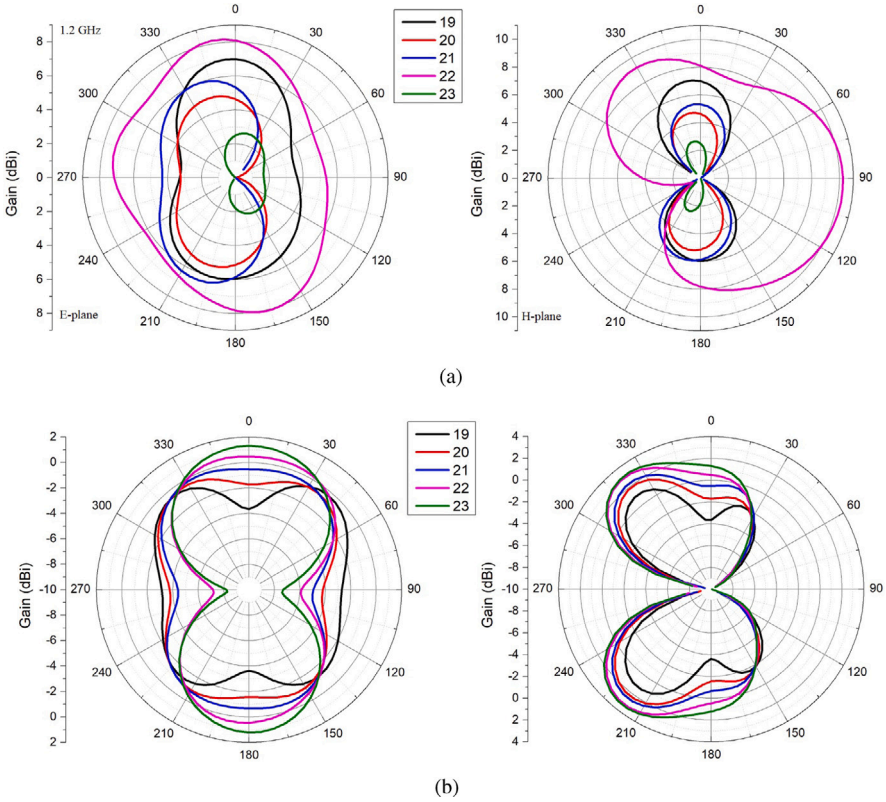

Fig. 7. Parametric analysis of ground stub length on radiation pattern (a) 1.2 GHz (b) 3.5 GHz.

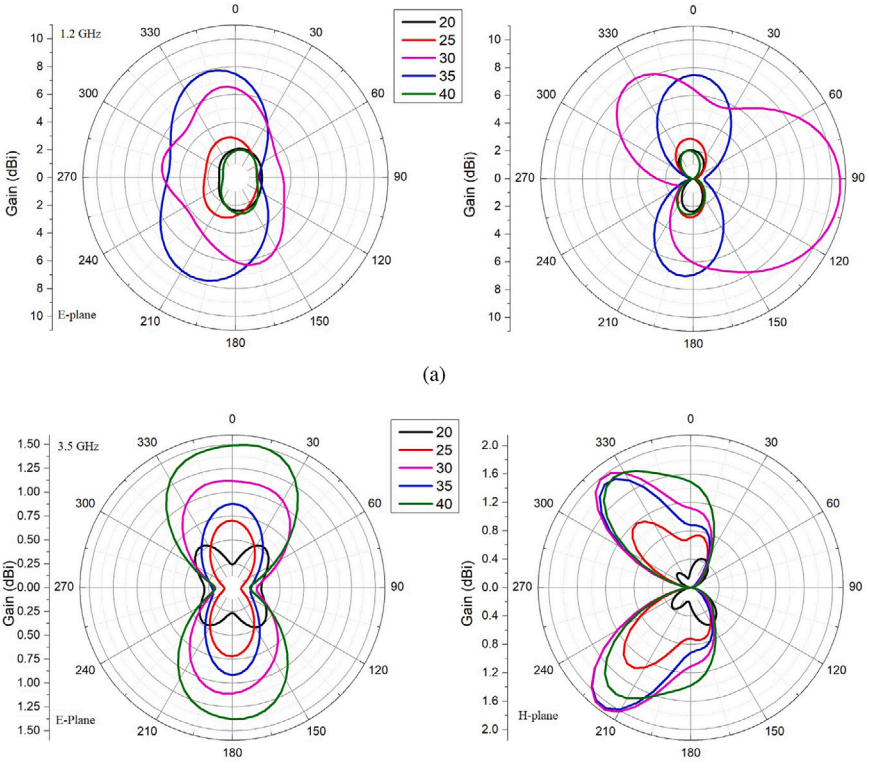

Fig. 8. Parametric analysis of ground stub position on radiation pattern (a) 1.2 GHz (b) 3.5 GHz.

Table 2
Comparison table.

Ref. No.	Conductive material/Technique	Substrate	Operation	Frequency band	Transparency (%)	Efficiency
[2]	Ion-exchange	Transparent	Narrowband	2.4 GHz	NA	NA
[4]	Metal mesh	Opaque	Dual band	1.6, 2.4 GHz	NA	56.44
[5]	Fluorine doped oxide	Opaque	Wideband	2–6 GHz	NA	28
[6]	Indium–zinc–tin oxide	Transparent	Narrowband	2.4 GHz	81.1	40
[7]	Metal mesh	Transparent	UWB	0.78–20 GHz	72	NA
[8]	Metal mesh	Transparent	Narrowband	2.4 GHz	80	66.32
[11]	Silver grid layer	Transparent	Wideband	2.1 GHz	70.7	85
[15]	AgHT-4	Transparent	Wideband	2.21–6 GHz	70	41
[16]	AgHT-8	Transparent	Dual band	2.27, 3.61 GHz	80	88
This work	ITO-PET	Transparent	Dual band	1.6, 3.25 GHz	>83	45.13

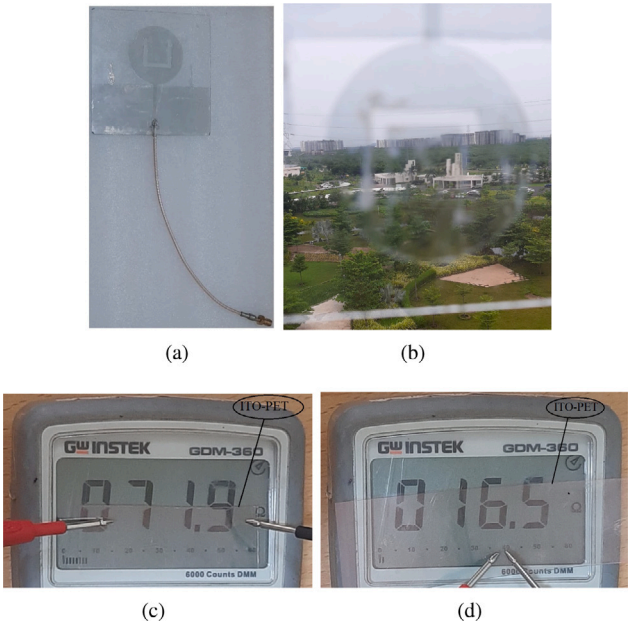

Fig. 9. Fabrication of the proposed antenna (a) Prototype of the ITO-PET based antenna. (b) Transparency of antenna through room window in day light. (c) Surface resistance at 40 mm probe distance. (d) Surface resistance at 3 mm probe distance.

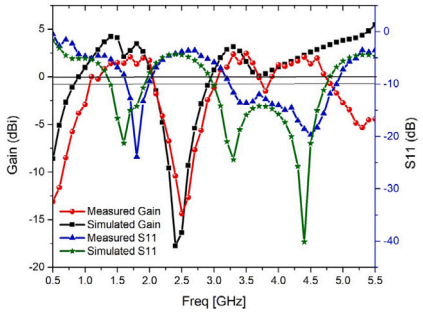

Fig. 10. Comparison of simulated and measured S11 and Gain.

oxide (SnO_2), offers both electrical conductivity and visible light transparency. PET, a flexible polymer with mechanical strength, combines with ITO through techniques like physical vapor deposition. ITO-PET excels in optoelectronic domains, with exceptional transparency, enabling its use in displays, touchscreens, and photovoltaics. The ITO layer imparts electrical conductivity to PET, making it suitable for electronic components. Its flexibility, even after mechanical stress, suits wearable electronics and curved displays. ITO-PET finds applications in transparent conductive films, touchscreens, electromagnetic shielding, smart windows, and photovoltaics. However, challenges include indium's cost, PET brittleness, and stability concerns. Further, a transparent soda lime glass of thickness 2 mm dielectric constant of 2.5 mm and dielectric loss tangent of 0.002 is used as a substrate. SLG is a widely favored material in electronic substrate applications. It primarily consisting of silicon dioxide (SiO_2), sodium oxide (Na_2O), and calcium oxide (CaO). SLG demonstrates impressive dielectric qualities, including a high dielectric constant and low loss tangent, making it invaluable for insulating layers in integrated circuits and PCBs. While challenges exist in achieving desired flatness and managing thermal expansion mismatches, SLG's contributions are pivotal in propelling advanced electronic device and system development.

The prototype under development, along with details regarding its transparency and conductivity, is visually presented in Fig. 9. The antenna, which is based on both ITO-PET and SLG technologies, is fed through a 50 Ω transmission line, as illustrated in Fig. 9(a). To establish connectivity, the transmission line's core and ground are affixed to the ITO-PET radiator and ground using Silver Epoxy Conductive Adhesive, a compound created by amalgamating silver particles with an epoxy resin matrix. This adhesive serves the dual purpose of bonding components and facilitating electrical conduction. Notably, challenges arise concerning stress management due to disparities in thermal expansion coefficients, demanding the pursuit of steadfast conductivity and adhesion uniformity. Moreover, the adhered sections are coated with a transparent adhesive to enhance mechanical strength. The transparency of the finalized prototype is vividly demonstrated in Fig. 9(b), wherein an outdoor image captures the antenna in front of a camera. It is discernible that the prototype boasts nearly seamless transparency, although slight haziness may arise due to the adhesive employed for the ITO-PET and SLG attachment.

The Figs. 9(c) and 9(d) presents the surface resistance characteristics of the ITO-PET sheet, specifically at two distinct probe distances: 40 mm and 3 mm, respectively. These figures unveil that the sheet manifests a surface resistance of 70.9 Ω when the probing distance is set at 40 mm. This resistance value undergoes a substantial reduction, plummeting to 16.5 Ω when the probe distance is constricted to a mere 3 mm. It confirms that the optically transparent ITO-PET sheet is sufficiently conductive and may be used for antenna fabrication. It becomes evident that the ITO-PET sheet possesses the requisite electrical characteristics to effectively facilitate the realization of antennas, thereby marking a significant stride in the realm of transparent and conductive materials for advanced technological applications.

The simulated results of the proposed antenna is compared with the measured results of the prototype and presented in Fig. 10. The measurement of the antenna is performed using method suggested in [18]. The antenna is developed using unconventional materials those are not exactly meant for the electronics and microwave applications. Thus a marginal variations in simulated and measured results are observed. The simulated and measured scattering parameter, realized gain and E and H-plane radiation patterns are shown in Fig. 10. The measured S11 parameter exhibits narrow bandwidth in both operating bands. In addition, the impedances matching is comparatively poor in the higher frequency band. However, the measured results confirms a dual band response with one narrow and another wideband operations in low UHF

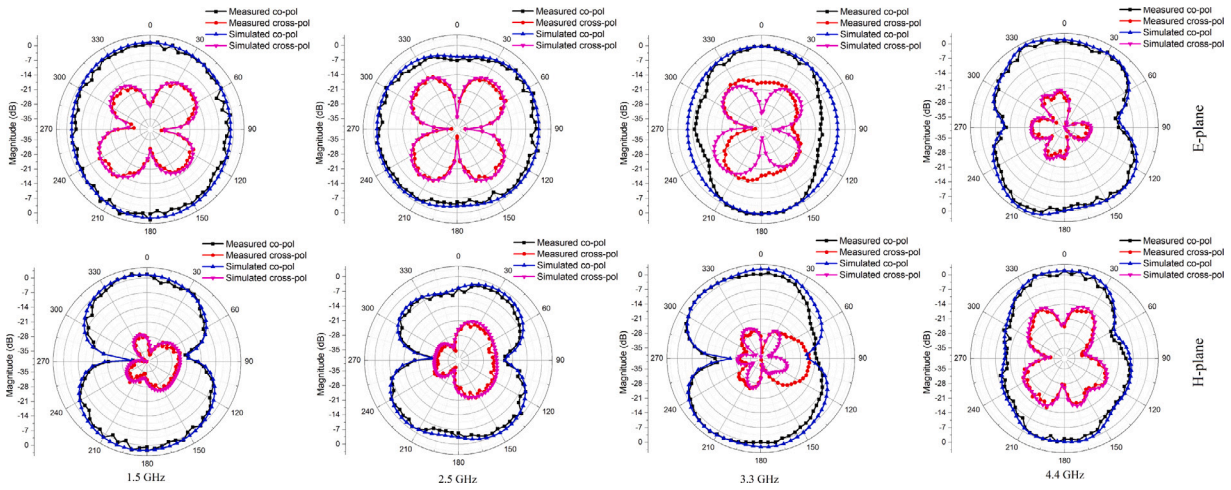

Fig. 11. Simulated and measured E and H-plane radiation pattern at 1.5, 2.5, 3.3 and 4.4 GHz.

and S-band, respectively. The measured gain of the antenna is positive in both operating bands, as shown in Fig. 10. In the low frequency band the antenna exhibits quiet a low gain due to many practical loss such as connector loss, pasting issue, and material impurity. In the high-frequency band the antenna has a slight upward shift in gain due to the shift of measured operating band. The E and H-plane radiation pattern at different operating frequencies are shown in Fig. 11. Co-polarization pattern has a good agreement between simulated and measured results for all operating bands for E as well as H-planes. However, as the cross-polarization power level is very low, its accurate measurement is a complex process thus a little more variation between simulated and measures results are observed. However, the co and cross polarization level have sufficient isolation making this antenna usable for the communication systems. The simulated radiation efficiency of the antenna is above 42.51% in both operating bands. In the lower and upper operating bands the antenna radiation efficiency is 43.51% and 45.13%, respectively. However, the radiation efficiency is reasonable for the consumer electronics applications.

A comparative analysis of the proposed antenna with some latest contributions in the literature is compared in Table 2. The optically transparent antennas are in developing stage and many successful designs using different conductive materials have been implemented. The proposed antenna has a comparable performance as evident in Table 2 which ensures the successful implementation of the design.

4. Conclusion

This article introduces an inventive optically transparent antenna, fashioned from Indium Tin Oxide-coated Polyethylene Terephthalate (ITO-PET) and Soda-lime-glass (SLG) substrates. The exploration of ITO-PET and SLG for transparent antenna construction is a central focus, including a thorough evaluation of the antenna's performance in relation to ITO-PET's conductivity. Operating seamlessly across dual bands, the antenna features a cleverly designed slotted circular structure with an enhanced ground plane. Despite ITO-PET's modest conductivity, the antenna surpasses expectations, showcasing a wider bandwidth in the higher frequency band and positive gain across both bands. The fabrication and precise measurement of the antenna prototype solidify the realization of this visionary concept, heralding a new era in transparent antenna technology with vast potential.

CRediT authorship contribution statement

Eknath C. Patil: Conceptualization, Methodology, Software, First draft. **Shashikant D. Lokhande:** Supervision. **Uday A. Patil:** Data curation, Writing – original draft. **Atula U. Patil:** Visualization, Investigation. **Jayendra Kumar:** Validation and prototyping.

Declaration of competing interest

The authors declare that they have no known competing financial interests or personal relationships that could have appeared to influence the work reported in this paper.

Data availability

No data was used for the research described in the article.

References

[1] S.-H Park, C.-K Park, H Yoo, B Kim, C.-B. Chae, Window-type and AR glass-type transparent antenna systems for B5G/6G, in: 2023 IEEE 20th Consumer Communications & Networking Conference (CCNC), Las Vegas, NV, USA, 2023, pp. 937–938, http://dx.doi.org/10.1109/CCNC51644.2023.10059609.

[2] TQ. Trung, NE. Lee, Flexible and stretchable physical sensor integrated platforms for wearable human-activity monitoringand personal healthcare, Adv. Mater. 28 (22) (2016) 4338–4372, http://dx.doi.org/10.1002/adma.201504244, Epub 2016 Feb 3. PMID: 26840387.

[3] Xinxing Xia, Frank Yunqing Guan, Yiyu Cai, Nadia Magnenat Thalmann, Challenges and advancements for AR optical see-through near-eye displays: A review, Front. Virtual Real. 3 (2022) http://dx.doi.org/10.3389/frvir.2022.838237.

[4] Y. Morimoto, S. Shiu, I.W Huang, E. Fest, G. Ye, J. Zhu, Optically transparent antenna for smart glasses, IEEE Open J. Antennas Propag. 4 (2023) 159–167, http://dx.doi.org/10.1109/OJAP.2023.3238721.

[5] Potti Devisowjanya, Mohammed Gulam Nabi Alsath, Savarimuthu Kirubaveni, G. Sudhilaya, Design and development of optically transparent rectenna for RF energy harvesting applications, 14 (8) (2022) 1081–1085. http://dx.doi.org/10.1017/S1759078721001616.

[6] S Hong, S.H Kang, Y Kim, C.W. Jung, Transparent and flexible antenna for wearable glasses applications, IEEE Trans. Antennas and Propagation 64 (7) (2016) 2797–2804, http://dx.doi.org/10.1109/TAP.2016.2554626.

[7] B Wu, X.-Y Sun, H.-R Zu, H.-H Zhang, T. Su, Transparent ultrawideband halved coplanar vivaldi antenna with metal mesh film, IEEE Antennas Wirel. Propag. Lett. 21 (12) (2022) 2532–2536, http://dx.doi.org/10.1109/LAWP.2022.3200455.

[8] S Hong, Y Kim, C. Won Jung, Transparent microstrip patch antennas with multilayer and metal-mesh films, IEEE Antennas Wirel. Propag. Lett. 16 (2017) 772–775, http://dx.doi.org/10.1109/LAWP.2016.2602389.

[9] S.H Kang, C.W. Jung, Transparent patch antenna using metal mesh, IEEE Trans. Antennas and Propagation 66 (4) (2018) 2095–2100, http://dx.doi.org/10.1109/TAP.2018.2804622.

[10] S Hakimi, S.K.A Rahim, M Abedian, S.M Noghabaei, M. Khalily, CPW-fed transparent antenna for extended ultrawideband applications, IEEE Antennas Wirel. Propag. Lett. 13 (2014) 1251–1254, http://dx.doi.org/10.1109/LAWP.2014.2333091.

[11] J Hautcoeur, F Colombel, M Himdi, X Castel, E.M. Cruz, Large and optically transparent multilayer for broadband H-shaped slot antenna, IEEE Antennas Wirel. Propag. Lett. 12 (2013) 933–936, http://dx.doi.org/10.1109/LAWP.2013.2274033.

[12] H.A Elmobarak Elobaid, S.K Abdul Rahim, M Himdi, X Castel, M. Abedian Kasgari, A transparent and flexible polymer-fabric tissue UWB antenna for future wireless networks, IEEE Antennas Wirel. Propag. Lett. 16 (2017) 1333–1336, http://dx.doi.org/10.1109/LAWP.2016.2633790.

[13] O.R Alobaidi, P Chelvanathan, B Bais, K Sopian, M.A Alghoul, Md. Akhtaruzzaman, N. Amin, Vacuum annealed Ga:Zno (GZO) thin films for solar cell integrated transparent antenna application, Mater. Lett. 304 (130551) (2021).

[14] A Desai, M Palandoken, J Kulkarni, G Byun, T.K. Nguyen, Wideband flexible/transparent connected-ground MIMO antennas for sub-6 GHz 5G and WLAN applications, IEEE Access 9 (2021) 147003–147015, http://dx.doi.org/10.1109/ACCESS.2021.3123366.

[15] Arpan Desai, et al., Transparent conductive oxide-based multiband CPW fed antenna, Wirel. Pers. Commun. 113 (2020) 961–975.

[16] Arpan Desai, et al., Dual band slotted transparent resonator for wireless local area network applications, Microw. Opt. Technol. Lett. 60 (12) (2018) 3034–3039.

[17] M Shahpari, D.V. Thiel, The impact of reduced conductivity on the performance of wire antennas, IEEE Trans. Antennas and Propagation 63 (11) (2015) 4686–4692, http://dx.doi.org/10.1109/TAP.2015.2479241.

[18] J Kumar, B Basu, F.A Talukdar, A. Nandi, Graphene-based wideband antenna for aeronautical radio-navigation applications, J. Electromagn. Waves Appl. 31 (2046) (2017) 18–2054, http://dx.doi.org/10.1080/09205071.2017.1359686.